Knocking down *MEG3* long non-coding RNA to Counteract Necroptosis *in vitro*

Contents

- Introduction
  i. Long non-coding RNAs
  ii. *MEG3*
  iii. Improved Alzheimer's Mouse Model and Findings
  iv. Necroptosis
  v. *MEG3* activates necroptosis in neurons
  vi. *MEG3* knockdown inhibits necroptosis activation
  vii. Thesis and Research aims
- Methods
- Results
  i. First gapmer assay for knocking down *MEG3*
  ii. Second gapmer assay targeting Exon 3 of *MEG3*
  iii. Dose-dependent Analysis of Gapmer-Mediated *MEG3* Silencing
  iv. Testing successful sequences in siRNA chemistry
  v. Necroptosis induction in vitro
  vi. Testing necroptosis inhibition through *MEG3* knockdown
- Discussion
  i. Discussion of Research and implications
  ii. *MEG3* upregulation in Cardiac disease
  iii. Limitations of research and future work
  iv. *MEG3* downregulation in cancer
  v. Distinct transcript variant targeting of *MEG3*
- Conclusion
- References
- Figures and Tables
  i. Table 1
  ii. Table 2
  iii. Table 3
  iv. Figure 1
  v. Figure 2
  vi. Figure 3
  vii. Figure 4
  viii. Figure 5

Introduction

The central dogma of molecular biology was defined in the late 1950's by the pioneering work of Francis Crick; it describes the one-way transfer of genetic information, progressing from DNA to RNA and then to protein *(1).* This idea of transcription and translation controlling the processes of genetic data was necessary to understand the fundamentals of complex cellular processes, but it does not explain the intricate system as a whole. Specifically, protein encoding genes only make up approximately 2% of the human genome *(2)*. Beyond this small fraction of protein-coding genes, the remaining 98% of the genome consists of non-coding regions, which regulate gene expression, chromatin structure, and cellular function (2, 3). Within these non-coding regions, further studies have categorized them into groups such as microRNAs (miRNAs), small interfering RNAs (siRNAs), enhancer RNAs (eRNAs), and long non-coding RNAs (lncRNAs), among others (3). These regulatory elements influence and coordinate the genome's output, playing a crucial role in shaping the central dogma and determining a cell's fate. The intricate and diverse functions of lncRNAs within this regulatory network are of particular interest in this study.

First believed to be just transcriptional noise, work on *H19* and *Xist* revolutionized our understanding of lncRNAs and a global effort to identify and characterize lncRNAs started at the turn of the millennium (*4, 5*). This coincided with the work of Hahn, M. W., and Wray, G. A. (2002), whose paper, *The G-value Paradox*, argued that an organism's complexity is determined not by the number of protein-encoding genes but by the intricate regulatory elements that control gene expression (6). Since then, over 100,000 lncRNA genes have been discovered in the human genome. These RNA molecules control various essential functions within the cell including gene regulation, RNA processing, molecular scaffolding, post-transcriptional control, and nuclear organization (*7*). By orchestrating these diverse cellular processes, lncRNAs play a critical role in maintaining cellular homeostasis. Therefore, as is the case with all biological machinery, dysfunctional activity of lncRNAs can be destructive to the cell, being associated with various diseases such as cardiovascular disease, neurological disorders, autoimmune disease, and cancer. One lncRNA of interest is Maternally expressed gene 3 (*MEG3*), whose dysfunction has been associated with numerous diseases.

MEG3 is an imprinted lncRNA found in the q32 region of chromosome 14. *MEG3* expression is regulated by two differentially methylated regions (DMRs): the intergenic DMR and the *MEG3* DMR (*8*). These DMRs play a critical role in controlling the expression of the DLK1-*MEG3* locus. Methylation at these regions leads to the repression of *MEG3*, while demethylation allows for its expression. When *MEG3* is expressed, it binds to the Polycomb Repressive Complex 2 (PRC2), which inhibits the expression of DLK1 [Figure 1b]. Methylation of the locus is found only on the paternal allele, so *MEG3* is only expressed on the maternal

allele hence the name, maternally expressed (*8, 9*). As is typical with lncRNAs, *MEG3* has a diverse transcriptome with nineteen known transcript variants and thirteen exons. Although there is variation in splicing patterns between each transcript variant, there is some conservation with exons 1, 2, 3, 10, 11 and 13 being found in all variants of *MEG3*. These six exons set the foundation for the lncRNA and then splicing variation controls the inclusion or exclusion of the seven other exons to produce a diverse array of *MEG3* transcript variants (*10*) [Figure 1a]. The specific role of each variant is unknown however, it is known that *MEG3* is a nuclear retained lncRNA and not found in the cytoplasm (*8*).

MEG3 plays a broad role in regulating gene expression through various pathways. One of its key functions is in chromatin remodelling and as previously mentioned it controls the imprinting of the DLK1-*MEG3* locus by binding PRC2. Additionally, *MEG3* can interact with Enhancer of Zeste Homolog 2 (EZH2), a component of PRC2, to suppress the expression of specific genes. When *MEG3* is upregulated, this interaction can lead to disease as *MEG3* binding to EZH2 inhibits the expression of Integrin Subunit Alpha 4 (*ITGA4*). *ITGA4* is crucial for endothelial cell functions such as adhesion, migration, and vascular remodelling. The interaction between *MEG3* and EZH2 leads to the enrichment of H3K27me3, a repressive histone modification, at the *ITGA4* promoter, inhibiting its expression [Figure 1c]. When *MEG3* is upregulated in endothelial cells, *ITGA4* expression is repressed stopping angiogenesis leading to vascular diseases associated with cardiac and peripheral ischemia (*11*).

MEG3 can also function as a competing endogenous RNA (ceRNA). In the case of miR-181, *MEG3* performs as a tumour suppressor and its loss of function in controlling miR-181 activity has been found to be a cause of gastric cancer. MiR-181 is a miRNA which regulates the expression of Bcl-2, a gene necessary in cell death. In a healthy cell, stable *MEG3* expression competes with Bcl-2 for miR-181 binding, allowing for the production of Bcl-2 to control programmed cell death and maintain cellular homeostasis. However, in gastric cancer, *MEG3* expression is downregulated, meaning miR-181 only binds Bcl-2, reducing its expression and stopping the tumour cells from dying, letting them grow and divide uncontrollably (*12*) [Figure 1c]. On the other hand, an example when upregulation of *MEG3* acting as ceRNA contributes to disease is in ischemic stroke. In healthy cells, *MEG3* can bind to the microRNA miR-21 but cannot outcompete the gene that miR-21 regulates, which is Programmed Cell Death 4 (PDCD4). This regulation allows for PDCD4 expression only when necessary. However, when *MEG3* is upregulated, it competes more effectively with PDCD4, reducing the binding of miR-12 to PDCD4, leading to its increased expression and heightened levels of apoptosis [Figure 1c]. This cascade of cell death is observed in ischemic stroke, contributing to significant neuronal cell loss (13).

The canonical function of *MEG3* is binding transcriptional factors to modulate their activity. In this example, *MEG3* interacts with p53, modifying its transcriptional activity selectively. For example, *MEG3* binding to p53 selectively enhances the transcription factors binding to the GDF15 promoter, leading to increased GDF15 expression. However, this interaction stops p53 from binding

other promoters such as p21CIP1 [Figure 1c]. This suggests that *MEG3* modulates p53's function, guiding it to activate certain genes over others. This selective activation shows that *MEG3* fine-tunes p53's activity rather than broadly stabilizing and activating all its targets. This fine tuning is necessary for cells in activating transcription programmes to regulate cell cycle, arrest, and death and therefore loss of this regulation can lead to cancer (*14*). These examples of *MEG3*'s diverse functions, along with the potential consequences of its dysregulation, underscore its critical biological importance as, particularly in unravelling the mechanisms driving various diseases. This relevance is further underscored by recent findings in an Alzheimer's model, where upregulation of *MEG3* was observed, suggesting a complex role for this lncRNA in the neurodegenerative process.

Alzheimer's disease (AD) is the most prevalent neurodegenerative disorder globally, with the number of affected individuals projected to double by 2050 (*15*). AD typically begins with subtle memory loss and cognitive decline, gradually progressing to more severe symptoms such as dementia (*16*). Despite the global impact of AD, it is still not a well understood disease lacking any beneficial treatment. One of the great drawbacks upon AD therapeutics is the lack of suitable models which accurately mimics the pathology found in humans. Currently 98% of drugs taken to clinical trials fail, due to the lack of conservation of disease pathology from animal models to humans (*17, 18*). By xenografting H9-derived human cortical neuronal progenitor cells (NPCs) into immunodeficient $Rag2^{-/-}$ adolescent mice, De Strooper, B., et al. recently provided a novel insight into the cellular mechanisms that lead to neurodegeneration in AD (*19*). The researchers xenografted two sets of NPCs, one set without any known AD mutations and the other with known familial AD mutations: Swedish mutation, Arctic mutation, and Iberian mutation. These three mutations increase amyloid beta production, amyloid plaque formation, and the production of the toxic Aβ42 peptide. After 6 and 18-months the mice with the mutated human-derived NPCs showed typical human AD: amyloid plaque formation, Tau fibril formation and phosphorylation, increased levels of soluble p-tau181 and p-tau231 as well as increased degeneration. These changes were observed exclusively in human neurons, highlighting the distinct differences in the susceptibility of human and mouse cell types to developing authentic Alzheimer's disease pathology.

Using this model the researchers looked at the gene expression of the AD affected neurons and compared them to the healthy control to understand the transcriptome differences which may cause degeneration. They identified 36 up-regulated and 21 down-regulated lncRNAs six months post xenografting. Of these lncRNAs, the one with the greatest difference in expression was *MEG3* which had a 10-fold upregulation compared to the control. Using in situ hybridization combined with cell-specific immunohistochemical markers they found that *MEG3* has a much greater enrichment in the nucleus of AD neurons. As well as *MEG3* upregulation, they found through quantitative polymerase chain reaction (qPCR) that necroptosis genes RIPK3 and MLKL also had a significant increase. This was further solidified using by staining the tissues with antibodies which target the phosphorylated states of the necrosome proteins p-RIPK1, p-

RIPK3 and p-MLKL. These findings add to previous studies that neurodegeneration in AD occurs though necroptosis (19).

Necroptosis is a form of programmed cell death and has distinct morphological features such as cell and organelle swelling, membrane rupture, release of damage-associated molecular patterns (DAMPS), and inflammation (*20, 21, 22*). Necroptosis initiation occurs through cytokines, Tumour Necrosis Factor-alpha (TNF-α) being the best studied, and pattern recognition receptors. Upon TNF-α binding, it is not a definite that necroptosis will be induced as the cell can form various complexes which determines the cells fate with complex formation being determined by the state of the cell upon binding (*21, 22*). The first complex, complex 1, is composed of TNF Receptor-Associated Death Domain Protein (TRADD), TNF Receptor-Associated Factor 2 (TRAF2), Cellular Inhibitor of Apoptosis Proteins 1 and 2 (cIAP1/2), Receptor-Interacting Protein Kinase 1 (RIPK1), Transforming Growth Factor Beta-Activated Kinase 1 (TAK1), the Linear Ubiquitin Chain Assembly Complex (LUBAC), and IκB Kinase (IKK). This mechanism leads to the activation of NF-κB signalling which causes the expression of proinflammatory genes. This cascade requires the ubiquitination of RIPK1, and the inhibition of this ubiquitination can lead to the complex II being formed. Complex II is split into two subgroups, complex IIa which lead to apoptosis and complex IIb which leads to necroptosis. Complex IIa occurs through the activation of caspase-8 which activates downstream caspases leading to apoptosis. It is required for apoptosis that capspase-8 is cleaved to the smaller 18-kDa subunit to activate the downstream cascade leading to cell death, the longer p43 subunit is inactive (*22*). On the other hand, if caspase-8 is inhibited or inactive, complex IIb will form, making necroptosis a caspase-independent cell death pathway. Complex IIb relies in the formation of the necrosome which consists of three proteins RIPK1, RIPK3 and MLKL. RIPK1 and RIPK3 are activated in the necrosome by autophosphorylation forming a large amyloid-like structure. RIPK3 recruits and phosphorylates MLKL causing MLKL to change shape leading to MLKL oligomerization. The oligomerized MLKL then moves to the plasma membrane, where it induces membrane rupture by forming pore clusters or regulating ion channel flux. This membrane rupture results in the release of damage-associated molecular patterns (DAMPs) and other intracellular contents into the extracellular space, which can trigger a strong inflammatory response, a contributor to disease pathogenesis (*21, 22, 23*). The upregulation of these necrosome proteins in the De Strooper., et al., (2023) AD mouse model alludes that complex IIb is being formed and causing degeneration in AD neurons.

To further investigate the effects of *MEG3* upregulation on neuronal cells, De Strooper., et al., transduced H9 human-derived neuronal cells with a *MEG3*-expressing lentivirus in vitro. The upregulation of *MEG3* was 10-fold, matching the levels observed in the AD mouse model, and resulted in a 40% increase in cell death after 11 days compared to cells transduced with a control lentivirus. To confirm that *MEG3*-induced cell death was driven by necroptosis, the researchers repeated the experiment but now treating the cells with three necroptosis inhibitors: ponatinib, dabrafenib, and necrosulfonamide. Treatment with these

inhibitors rescued the cells from *MEG3*-induced cell death, with survival rates equal to or greater than that of the control group. This demonstrated that *MEG3* upregulation activates necroptosis in neuronal cells. Next, the researchers translated these findings to the AD mouse model by knocking down *MEG3* expression using a short hairpin RNA (shRNA). Mice treated with the *MEG3* targeting shRNA exhibited a higher neuronal cell count compared to those treated with non-targeting shRNA. Additionally, the *MEG3*-knockdown group showed reduced levels of nuclear pRIPK1 in AD neurons. This data shows that *MEG3* upregulation drives cell death in the AD model and that knocking down *MEG3* can rescue these cells (*19*).

To further establish that necroptosis is the primary mechanism of cell death in AD, the researchers administered ponatinib and dabrafenib in the AD mouse model. Both inhibitors significantly reduced the levels of necroptosis markers, pRIPK1, pRIPK3, and pMLKL, and increased neuronal survival in the xenografted human neuronal cells. In addition, CRISPR-Cas9-mediated deletion of RIPK3 enhanced cell survival in the AD mouse model. Taken together, this data strongly supports the conclusion that neuronal degeneration in AD occurs through necroptosis and that *MEG3* upregulation activates this pathway. *MEG3* knockdown or pharmacological inhibitors can rescue cells in the AD model by inhibiting necroptosis (*19*).

MEG3 knockdown, as demonstrated by De Strooper et al., presents a promising therapeutic approach to reduce neuronal cell death in Alzheimer's disease, potentially alleviating the symptoms and slowing the progression of the condition. However, a clear issue in the shRNA method used by these researchers arises when taking a deeper look into diverse *MEG3* transcript variants. Firstly, in the paper they claim the transcript variant with accession number NR_002766.2 (referred here as Variant 2) is the most abundant in the AD human neurons. However, the shRNA they use, which was lifted from another paper (*24*), targets a non-abundant *MEG3* transcript variant at an exon, exon 12, found in only 4 of the 19-transcript variants [Figure 1a]. This is first issue I have with their method of targeting as they are not able to ubiquitously reduce *MEG3* expression based on the region in which they are targeting. Another issue is that they used a shRNA to mediate the knockdown. *MEG3* as mentioned before is nuclear retained lncRNA which performs its functions inside the nucleus. On the other hand, shRNAs work in the cytoplasm using RNA interference machinery. This discrepancy in location significantly reduces the timeframe for which *MEG3* can be knockdown as binding by the shRNA can only occur for the short period of time when the lncRNA undergoes post transcriptional modifications and splicing. If *MEG3* knockdown is going to progress as a therapeutic to alleviate cell death in AD a better knockdown method needs to be established.

To address this challenge, my research focuses on developing a more effective and reliable method for *MEG3* knockdown. I will first focus upon targeting regions of *MEG3* that are common to all transcript variants and choose an oligonucleotide chemistry that performs its knockdown in the nucleus. Upon testing various regions of *MEG3* I hope to find a sequence that is best to reduce

MEG3 expression. From here I wish to validate the findings of De Strooper., et al., that *MEG3* knockdown can rescue cells from necroptosis, showing that *MEG3* knockdown is a viable therapeutic avenue for inhibiting necroptosis in AD and potentially other diseases.

Methods

Gapmer design and synthesis

Note: The gapmers used in this experiment were not designed or synthesized by me. My previous supervisor, Francois Halloy, synthesized all gapmers used in my thesis. I am including the synthesis in my methods for completeness.

Gapmers targeting *MEG3* exons were designed to maximize overlap across multiple isoforms while minimizing off-target effects. Sequences were assessed for self-complementarity and specificity using BLAST. Each gapmer included DNA wings flanking a central RNA-like region with GC content optimized in necessary 40-60% range. All amidites used in this study were purchased from ChemGenes and prepared at a concentration of 0.1 M in dry acetonitrile (less than 15 ppm water content). The standard DNA amidites included dA, 5-methyl dC, dG, and dT, while the modified oligonucleotide amidites included MOE A, MOE 5-methyl C, MOE G, and MOE T. The synthesis was performed under an inert argon atmosphere. Reagents used included a 3% trichloroacetic acid (TCA) deblock solution in dichloromethane (Sigma Aldrich, Cat# L020000), 0.3 M benzylthiotetrazole (BTT) in dry acetonitrile as the activation reagent (ChemGenes, Cat# RN-1452), and DDTT solution (0.05 M) for sulfurization (ChemGenes, Cat# RN-1688). Capping solutions consisted of Cap A (ChemGenes, Cat# RN-1458) and Cap B (ChemGenes, Cat# RN-7776). Acetonitrile (Sigma Aldrich, Cat# L010000) was used for washing steps. Oxidation steps were not used during synthesis. Post-synthesis, oligonucleotides were cleaved from the solid support by incubating in 1 ml of 25% ammonia at 65°C for 8 hours. The cleavage solution was evaporated in a SpeedVac for 4 hours, concentrating the crude oligonucleotide to approximately 300 μl. LC-MS analysis confirmed that the oligonucleotides had a purity of 85-90%, sufficient for biological testing, and thus a single round of sodium-ethanol precipitation was used for purification. For precipitation, crude oligonucleotide solutions were mixed with 10X 0.3 M sodium acetate, pH 5.5, followed by the addition of 4 volumes of pure ethanol, which caused instant precipitation. The solutions were cooled overnight at -20°C and centrifuged at 12,500g for 15 minutes at 4°C. The supernatants were carefully removed and retained for potential reanalysis, while the pellets were washed with ice-cold 90% ethanol, centrifuged again, and briefly dried at room temperature. The pellets were then dissolved in 400 μl of RNase-free water and shaken at 1000 rpm for 30 minutes at room temperature. A final centrifugation at 13,000g for 15 minutes removed any remaining solid particles. The resulting supernatants, with a final volume of 350 μl, were transferred to fresh Eppendorf tubes, vortexed briefly, and prepared for analysis.

Cell culture and transfection

General cell culture protocol: SMA Type II patient fibroblasts (Coriell Institute GM03813) were grown in DMEM-Glutamax (Gibco 10564-011) supplemented with 10 % fetal bovine serum (Gibco A5256701) and 1 % Antibiotic/Antimycotic solution (Merck A5955). Cells were maintained at 37°C with 5% CO2 and passaged twice weekly using TrypLE Express (Gibco 12604013).

Gapmer transfection in fibroblasts: Cells were plated at 50,000 cells/well in 1ml of medium in a CytoOne 24-well plate (CC7682-7524). Gapmer transfection occurred 24hr after plating using Lipofectamine 2000 (Invitrogen 11668-027) in line with the manufacturers' instructions. Gapmers were diluted in 50ul Opti-MEM medium (Gibco 51985-047) prior to mixing with 49ul Opti-MEM containing 1ul of Lipofectamine 2000. Solutions were incubated at room temperature for 20 minutes before adding to cell culture medium. Total volume of gapmer treatment added was 100ul. All treatments were stopped after 36 hours.

IC50 transfection in fibroblasts: Cells were plated 20,000 cells/well in 400ul of medium in a CytoOne 48-well plate (CC7682-7548). The remainder of the procedure followed the same steps as the *Gapmer transfection protocol in fibroblasts*.

siRNA transfection in fibroblasts: The siRNAs were purchased from Integrated DNA Technologies. Cells were plated at 50,000 cells/well in 1ml of medium in a 24-well plate. siRNA transfection occurred 24hr after plating using RNAiMax (Invitrogen 13778-075) as per the manufacturers' instructions. siRNA was diluted in 50ul Opti-MEM medium prior to mixing with 47ul Opti-MEM containing 3ul of RNAiMAX. Remaining method is same as *Gapmer transfection in fibroblasts.*

Necroptosis induction: Cells were plated at 50,000 cells/well in 1ml of medium in a 24-well plate. The necessary volume of TNF-α was added for the required concentration in each well. TNF-α was incubated in each well for 6 hours before processing for analysis.

Necroptosis revival: Cells were plated at 50,000 cells/well in 1ml of medium in a 24-well plate. Untreated and TNF only wells were treated with 1ul of blank lipofectamine. Gapmer wells were transfected same as *Gapmer transfection in fibroblasts.* Wells were left for 30 hours before TNF-α was added and left in solution for 6 hours before stopping for analysis.

Off-target hit analysis

Oligo 12 was analysed for off-target hits using the GGGenome database. The sequence was searched against the "Human pre-spliced RNA, RefSeq curated on GRCh38/hg38.p14, D3G 24.03 (Mar, 2024)" dataset for complementary matches on the plus strand. Searches were conducted with 2, 3, and 4 mismatches to identify potential hits. Gene names corresponding to the matches were retrieved

from NCBI. For relevant genes, the genomic location of the match (intron or exon) was determined using NCBI's annotation tools.

RNA extraction and Reverse transcription

Cells were washed one time with 500 µl phosphate-buffered saline (PBS) and pelleted. RNA extraction was performed using the Qiagen RNEasy kit, following the manufacturer's instructions. cDNA was synthesized using the High-Capacity cDNA Reverse Transcription Kit (Applied Biosystems #4368814), with 400 ng of RNA as input. cDNA samples were diluted 1/5 (v/v) in RNase-free water prior to use in real-time PCR.

RT-qPCR

RT-qPCR reactions were prepared with the SYBR Green™ Gene Expression Master Mix (Applied Biosystems # 4369016) and run and analysed on the StepOnePlus™ real-time PCR system (Applied Biosystems). *MEG3, RIPK1, RIPK3, MLKL*, housekeeping *PolJ* and *GAPDH* were amplified using SYBR Green primers found in **Table1**. *PolJ* served as the reference control for *MEG3* quantification, while *GAPDH* was used for necrosome protein quantification. Each reaction was completed in duplicate. Fold changes were calculated using the ΔΔCt method. Untreated cells were used as calibrators.

Statistical analysis

Statistical significance was determined with a minimum of n = 3 biological replicates using BioRender software and one-way ANOVA tests with Dunnett's correction for figures 2, 4 and 5. Dose response linear regression was used for figure 3. Statistical comparisons were made to untreated cells. In cell culture experiments, data from independent replicates were combined with the value of the control group returned to 1 in each case. P values less than 0.05 were considered to be statistically significant. Statistical tests and error bars are detailed in figure legends.

Results

First gapmer assay for knocking down MEG3.

The first step of this study was to choose the most conserved regions of *MEG3* to target for knockdown. Using Ensembl genome browser and NCBI Refseq to look at *MEG3* exon architecture and transcript variation, it was clear that exons 2 and 3 were the best regions to target as these are conserved in all transcript variants of *MEG3* (Figure 1). The sequences of these two exons provided the backbone for oligonucleotide synthesis. An array of 12 gapmers

targeting these two exons was synthesized. None of the sequences from the array exhibited signs for self-complementation. While initial analysis did not reveal any obvious off-target hits, a more thorough investigation uncovered BLAST data indicating potential off-target interactions for Oligo 12 [Table 3]. Genes included in this table were selected based on post-analysis findings, focusing on whether their loss of function significantly impacted disease and if they were expressed in the central nervous system (CNS). All had GC content between 40-60% and melting temperatures (Tm) ranging from 65-75ºC [Table 1]. Synthesis and purification of these gapmers were successful, and they were prepared for *in vitro* testing.

Cells were treated with 250 nM of each gapmer, and activity was assessed 36 hours post-transfection by calculating relative expression of *MEG3* using negative control transfected cells as the calibrator and TBP as the endogenous house-keeping gene in qPCR. I observed effective knockdown activity in all gapmers with top performers Oligo1, Oligo8, Oligo9, and Oligo12 which reduced target expression to as low as 10% relative to the non-target control [Figure 2a]. Oligo1 targets the second exon and the latter four gapmers target exon 3. These results indicate that exon 3 is the most effective target for reducing *MEG3* expression. The next step is to explore additional sequences within exon 3 for gapmer targeting, aiming to identify a more effective sequence for downregulating *MEG3* expression.

Second gapmer assay targeting Exon 3 of MEG3.

Given the success of targeting exon 3 in the initial assay, I proceeded to perform a micro-walk along exon 3 to fine-tune the gapmer design for optimal efficacy in knocking down *MEG3* expression. Similar to the previous assay, these gapmers showed no off-target hits, lacked self-complementarity, and exhibited sufficient GC content and melting temperatures [Table 2]. The six gapmers previously designed to target exon 3 were tested again alongside 13 new gapmers that spanned the 5’ region, with slight nucleotide shifts between the sequences [Figure 2b]. After synthesis, these gapmers were transfected and tested using the same method as before. As shown in Figure 2b, targeting exon 3 proved highly effective in reducing *MEG3* expression. Out of the 19 gapmers tested, 14 reduced *MEG3* expression to 10% or less of the baseline level observed in negative control-treated cells. Notably, 9 of these gapmers achieved reductions below 5% of the control levels, indicating highly efficient knockdown. The most effective gapmers—Oligo8, Oligo9, Oligo12, Oligo13, and Oligo25—reduced *MEG3* expression to 3% or less relative to the negative control. On average, *MEG3* expression across all gapmers was reduced to 8.14% of the control level, with the control was set at 100%. This represents a 3.36% further reduction in *MEG3* expression compared to the average knockdown achieved in the previous assay. These findings highlight exon 3 as a robust target for achieving substantial *MEG3* knockdown. Given that three times as many gapmers were tested compared to the first assay, these results further

demonstrate the robustness of *MEG3* knockdown by gapmers targeting sequences within exon 3.

Dose-dependent analysis of Gapmer-Mediated MEG3 Silencing

A dose-dependent experiment was performed to assess the potency of Oligo1, Oligo8, Oligo9, and Oligo12 in reducing *MEG3* expression across nine concentrations (1 nM, 10 nM, 25 nM, 50 nM, 125 nM, 250 nM, 500 nM, 750 nM, and 1000 nM) over a 36-hour period. Expression levels were normalized to the negative control. Figures 3A–D, plotted on a consistent y-axis scale for comparison, show that all oligonucleotides induced dose-dependent reductions in *MEG3* levels, though with distinct response profiles. Oligo1 (Figure 3A) exhibited a sharp reduction between 10 nM and 50 nM, reaching maximal knockdown at 125 nM and plateauing beyond 250 nM. Similarly, Oligo8 (Figure 3B) demonstrated a steep decline in *MEG3* expression between 10 nM and 50 nM, achieving 90% knockdown by 100 nM, with no further decrease after 250 nM. In contrast, Oligo9 (Figure 3C) showed a more gradual dose-response, with significant reductions occurring from 25 nM to 125 nM and maximal knockdown at 500 nM. Oligo12 (Figure 3D) was the most potent, showing a strong reduction starting at 10 nM, with maximal knockdown achieved by 250 nM.

Projected dose-response graphs (Figures 3E–H) were generated to illustrate data trends at lower concentrations that were not tested experimentally, providing a better estimate of IC50 values. These projections suggest that all oligonucleotides likely have IC50 values in the low nanomolar range. Among the four gapmers, Oligo12 emerged as the most effective, demonstrating superior potency and achieving the most robust knockdown of *MEG3* expression. These findings highlight the dose-dependent activity of these gapmers and underscore Oligo12 as the leading candidate for *MEG3* silencing.

Testing successful sequences in siRNA chemistry

To corroborate my initial hypothesis that siRNA targeting of *MEG3* does not result in more efficient knock down compared to ASO, I sought to test the chosen sequence in siRNA. The chosen sequences taken to this stage of testing were Oligo1, Oligo9, and Oligo12. The negative control sequence was also bought and used as the calibrator in qPCR. The siRNAs were tested at three concentrations, 5 nM, 10 nM and 40 nM. The effects were also assessed at two timepoints: 36- and 72-hours post-transfection. Since the siRNA has not been previously tested, it is crucial to monitor how the knockdown progresses over multiple time points to gain a comprehensive understanding of the gene silencing kinetics.

At both timepoints only Oligo12 was able to knockdown *MEG3* expression significantly [Figure 4a]. A dose-dependent response was observed at both timepoints, with a 17.4% fold change in *MEG3* expression compared to control for both 36 hours and 72 hours. On average, *MEG3* expression was reduced slightly

more after 72 hours (19.6% of control levels) compared to 36 hours (23.5% of control levels) [Figure 4a]. There was no significant knockdown in *MEG3* expression for either Oligo 1 or 9. These results clearly indicate that Oligo12 is the most effective sequence for *MEG3* knockdown, therefore this sequence will be taken to the next stage of testing for necroptosis revival. Additionally, given the novelty of my finding, I proceeded to patent this sequence with the assistance of the Oxford University Innovation (OUI) Office.

Necroptosis induction in vitro

Necroptosis induction can vary between cell types and a clear, optimized method to induce necroptosis in fibroblast cells has not been defined. Therefore, I tested various concentrations and timepoints of TNF-α to activate necroptosis. The manufacturer recommends TNF working concentrations of 1-10 ng/mL. However, given the resilience of fibroblasts, I selected 10 ng/mL as the lowest concentration and tested higher doses of 20, 30, and 40 ng/mL. As well as testing various concentrations, I tested two timepoints 6- and 12-hours TNF transfection. At the 12-hour timepoint post-transfection, the cells showed clear signs of toxicity (e.g., detachment from the plate) therefore, I proceeded with the 6 hours timepoint. Untreated cells were used as control and GAPDH as the calibrator for qPCR with fold changes in the expression of RIPK1, RIPK3 and MLKL being analysed.

At 6 hours post-transfection of TNF, I observed a dose-dependent response of all three necrosome genes. There was a significant increase of MLKL at all concentrations however, this gradually increased up to 30 ng/mL where the response plateaued at over 300% [Figure 5c]. In contrast, the expression of RIPK1 and RIPK3 did not become significant until 30 ng/mL, where they increased and remained elevated at 40 ng/mL. [Figure 5a, b]. Despite the short exposure time and the inherent resilience of fibroblasts to stress, TNF successfully induced necroptosis *in vitro*, shown by changes in the expression of necrosome-related genes. This optimized method will aid the investigation of my final hypothesis.

Testing necroptosis inhibition through MEG3 knockdown

The final hypothesis of my research is that gapmer-mediated knockdown of *MEG3* will rescue cells from TNF-induced necroptosis by reducing necrosome expression compared to non-target control transfection. All the work leading up to this point has been necessary to address this research aim. First, I developed a method to knock down *MEG3* expression to 5% of the non-target control, while also optimizing conditions for inducing necroptosis in vitro. For the final experiment, cells were transfected for 30 hours with 250 nM of Oligo12, followed by treatment with 30 ng/mL of TNF-α for the final 6 hours [Figure 5d]. For controls I used: cells treated with only 1ul of lipofectamine; cells treated with 1ul of lipofectamine and 30 ng/mL TNF for 6 hours; and cells treated with 1ul of

lipofectamine, 30 ng/mL TNF for 6 hours and 250 nM of the non-target control (NTC) gapmer for 30 hours preceding the TNF. These conditions allowed me to normalise the fold changes of necrosome expression to untreated cells whilst comparing the effects of *MEG3* targeting and non-targeting gapmers to necroptosis-induced cells.

As expected from the previous experiment, TNF alone was able to increase necrosome gene expression significantly, in particular MLKL. This upregulation, however, was rescued by the transfection of Oligo 12 and surprisingly also the non-target control [Figure 5h]. Both Oligo 12 and NTC had the same effect significantly reversing the increased expression of the necrosome. This change was most pronounced in MLKL, where expression decreased from a 6-fold upregulation to 20% of untreated sample levels. However, this reduction was not statistically significant, as determined by ANOVA. Similar downregulation was observed for RIPK1 [Figure 5f] and RIPK3 [Figure 5f] but these two reductions were deemed significant using the same analysis with a P-value < 0.0001. Therefore, the hypothesis is rejected, as *MEG3* knockdown was able to rescue cells from necroptosis [Figure 5e]; however, the non-targeting ASO sequence produced a comparable effect.

Discussion

AD is a chronic neurodegenerative disorder which begins with neuronal loss in the hippocampus, spreading to cortical regions where higher cognitive functions become impaired. Alzheimer's disease pathology was traditionally centred around amyloid plaque formation as this was thought to be the primary cause of neurodegeneration (*25*). However, in recent years, the focus has shifted, with growing evidence suggesting that inflammation plays a central role in driving degeneration (*26*). The complexity of AD pathology has posed challenges for previous research, as developing a precise and reliable model that closely replicates human AD has proven difficult (*17, 18*). This is one of main reasons for our current lack of understanding about the mechanism of degeneration as well as inability to produce effective therapeutics. The model produced by De Strooper., et al., provides a gateway into understanding human AD. There work highlights two important findings; that degeneration in AD occurs through the necroptosis cell death pathway and that lncRNA *MEG3* is able to activate this pathway through overexpression (*19*). Therefore, therapies to target AD can take two separate routes, target necroptosis directly or stop the activator, *MEG3*. I decided to investigate the latter by optimizing *MEG3* knockdown as this was not well explored in the 2023 paper. This proved beneficial as all oligonucleotide therapies were able to significantly knockdown *MEG3* expression.

To enhance the knockdown of *MEG3*, I focused on two key areas for improvement. Firstly, I prioritized a chemistry that functions within the nucleus, as *MEG3* is localized there, and secondly, I targeted conserved regions of *MEG3* to ensure ubiquitous knockdown of expression. To address the first area, I chose gapmers, which operate in the nucleus by utilizing RNase H machinery to degrade RNA (27). Gapmer design was crucial to produce optimal oligonucleotides capable of binding and degrading *MEG3*. This involved designing

gapmers with a 40–60% GC content to ensure stable binding (28). They were engineered with a full phosphorothioate backbone to enhance stability within the cellular environment. The incorporation of 2′-O-methoxyethyl (2′-MOE) modifications in the RNA wings further improved stability and significantly increased binding affinity to the target RNA. Additionally, 5-methylcytosine modifications facilitated efficient hybridization of the gapmer to the complementary RNA sequence (29). The melting temperature (Tm) was optimized to remain between 65–75ºC, ensuring stable hybridization to the necessary *MEG3* region while reducing the likelihood of off-target binding. All gapmers fell within this Tm range, providing stable binding while minimizing the risk of off-target effects.

To evaluate the potential off-target effects of Oligo 12, I conducted an in-silico analysis using GGGenome to identify sequences with significant complementarity, as even short contiguous matches can induce RNase H-mediated RNA degradation (43, 44). Several genes with off-target binding potential were identified, summarized in [Table 3], with metrics such as binding site location, mismatches, and percentage identity. Among these, *GRM7*, *HNF4A*, *CACNA1A*, and *ESR1* were particularly relevant due to their essential biological roles and their involvement in disease when disrupted. *GRM7*, a metabotropic glutamate receptor highly expressed in the CNS, regulates synaptic signalling, and its dysregulation has been implicated in neuropsychiatric disorders such as depression and schizophrenia (45). *HNF4A*, though primarily expressed in the liver and pancreas, is critical for metabolic homeostasis, with mutations linked to diabetes (46). *CACNA1A*, encoding a voltage-gated calcium channel, is vital for neuronal excitability and synaptic transmission, with mutations associated with episodic ataxia and spinocerebellar ataxia (47). Lastly, *ESR1*, a nuclear receptor for oestrogen, plays a key role in oestrogen-regulated transcription and is implicated in diseases such as breast cancer and osteoporosis (48). Off-target hits on these genes could result in significant functional disruptions, potentially leading to severe metabolic, neurological, or oncological consequences, highlighting the importance of minimizing unintended effects in therapeutic development.

The distinction between intronic and exonic binding introduces differences in the time window during which Oligo 12 can act. Off-target binding within exons allows interaction at both the pre- and post-splicing stages of mRNA, extending the time during which knockdown could occur. In contrast, intronic binding is restricted to the pre-splicing stage, potentially shortening the window of action. All identified off-targets were located within introns apart from *HNF4A* which has exonic binding. To validate if Oligo 12 can bind and knockdown these genes experimentally, qPCR can be used to measure transcript levels of these genes, providing direct evidence of potential off-target effects. This approach ensures specificity while addressing the therapeutic safety of Oligo 12. These results emphasize the importance of understanding the molecular context of off-target interactions in oligonucleotide design.

For ubiquitous knockdown of *MEG3*, I targeted regions conserved across all transcript variants. By referencing RefSeq and Ensembl data, I selected sequences located in the second and third exons of *MEG3*. All gapmers from both assays demonstrated significant knockdown of *MEG3* expression. Compared to Zhang et al. (2019), my gapmers achieved greater efficacy, with the most effective gapmer reducing *MEG3* expression by over 30% more. This improvement is attributed to the optimized gapmer chemistry, strategic targeting of conserved regions in *MEG3*, and the careful evaluation of off-target interactions to maximize specificity.

The dose-dependent analysis revealed Oligo 12 as the most effective gapmer in the assay system, achieving significant *MEG3* knockdown at lower concentrations compared to Oligo 1, Oligo 8, and Oligo 9. Oligo 12 demonstrated a sharp dose-dependent reduction in *MEG3* expression starting at 10 nM, with maximal knockdown at 250 nM and no further reductions beyond this concentration. The consistent efficacy of exon 3-targeting gapmers, particularly Oligo 12, underscores the importance of this region for silencing MEG3. Achieving effective knockdown at lower concentrations is crucial, as it minimizes the risk of off-target effects, reduces toxicity, and decreases the likelihood of side effects, especially for chronic or long-term treatments. While Oligo 8 and Oligo 9 also exhibited substantial knockdown, they required higher concentrations to achieve similar effects, and Oligo1 displayed a steep but narrower dose-response. Beyond sequence selection, potency could be further enhanced by optimizing the chemical modifications of the gapmers, such as increasing backbone stability or incorporating locked nucleic acids (LNAs) to improve binding affinity and target specificity. Delivery strategies, such as conjugating gapmers to tissue-specific ligands or nanoparticles, could also be explored to maximize cellular uptake and therefore, potency of the gapmer meaning a reduced dose is required to produce therapeutic effects whilst minimising toxicity (49). These findings highlight the dose-dependent activity of these gapmers and establish Oligo 12 as the most promising candidate for further research.

The siRNA experiments confirmed that Oligo12 is the most promising candidate for patenting, as it was the only sequence consistently effective in knocking down *MEG3* across both chemistries tested. A somewhat surprising finding as siRNA tend to work within the cytoplasm and *MEG3* is a nuclear localised lncRNA, again possibly suggesting that this sequence is highly effective (*8*). Oligos 1 and 9 showed no effect on *MEG3* expression, which is expected due to differences in their cellular localization of the lncRNA and RNA interference machinery. However, Oligo 12 was able to bind and reduce expression, despite the limited window of activity. The knockdown would occur when the lncRNA goes to the cytoplasm for post transcriptional modifications. In addition to evaluating different siRNA sequences, this experiment also assessed various time points and concentrations. Observing the effects at different intervals allows us to determine the onset, peak efficiency, and duration of gene silencing. This approach helps determine the optimal time point for achieving maximum knockdown, ensures the silencing effect is sustained, and provides valuable insights into the overall efficacy and stability of the siRNA treatment. The results

clearly indicated that Oligo12 was the ideal candidate for patenting due to its functionality in both gapmer and siRNA assayss. Since this finding was significant enough to guide our decision to patent Oligo12, it is essential to confirm that the observed *MEG3* knockdown is not an artifact. To validate this, I would test Oligo12 in a cell line with loss-of-function mutations in the Ago2 protein, which is responsible for cleaving mRNA upon siRNA binding. If *MEG3* expression is not reduced in this mutant cell line, it would confirm the efficiency of Oligo12 as an siRNA.

Necroptosis induction has been extensively studied, particularly in the context of TNF-α binding to the TNF1 receptor, leading to necrosome formation when RIPK1 is deubiquitinated and caspase-8 is inactive (22). While the literature suggests that combining TNF-α with a caspase-8 inhibitor, Z-VAD-FMK, can reliably induce necroptosis in vitro (20), my experiments in fibroblast cells revealed that TNF-α alone was sufficient to upregulate necrosome genes. Interestingly, the incorporation of Z-VAD-FMK did not significantly enhance this effect, suggesting that fibroblast cells may exhibit unique necroptosis dynamics. To evaluate necroptosis rescue mediated by *MEG3* knockdown, I focused on the relative expression of necrosome genes, a well-established metric in AD-related studies (19, 30).

Although Oligo12 effectively knocked down *MEG3* expression, necrosome expression was similarly rescued in cells treated with the non-targeting control (NTC) gapmer, indicating potential confounding factors. One possibility is that the high concentration of gapmers (250 nM), combined with a strong dose of TNF-α (30 ng/mL), may have triggered cell death through alternative pathways, complicating the interpretation of necroptosis-specific rescue. Another explanation could be unintended interactions between the NTC and the necroptosis pathway. While testing an additional NTC sequence could have clarified this, time constraints prevented further exploration. These findings, consistent with De Strooper et al., work in showing that *MEG3* knockdown influences necroptosis-related genes, underscore the need for refined experimental designs to isolate the specific role of *MEG3* in necroptosis rescue.

Although promising, the therapeutic potential of targeting *MEG3* in AD must be critically assessed. Despite the work of De Strooper et al., it remains unclear whether *MEG3* upregulation is a driving force in AD pathology or a secondary consequence of neurodegeneration. Additionally, the timing of *MEG3* dysregulation relative to disease onset is uncertain, potentially limiting its utility as a therapeutic target if upregulation occurs late in the disease process. The complex pathology of AD, encompassing amyloid-beta accumulation, tau aggregation, oxidative stress, and inflammation, further suggests that *MEG3* may not play a significant role in all cases. Moreover, differences between experimental models and human disease could mean that *MEG3* dysregulation observed in models is not fully representative of its behaviour in AD patients. These uncertainties highlight the need for further research to clarify *MEG3*'s role in AD and evaluate its viability as a therapeutic target.

As previously discussed, *MEG3* is a complex lncRNA with diverse functions, and its dysregulation has been implicated in a range of diseases. Notably, *MEG3* upregulation has been strongly associated with cardiac disease (*32, 33*). The first cardiac disease in which *MEG3* upregulation contributes is acute myocardial infarction (AMI). AMI is caused by acute and persistent ischemia, along with hypoxia in the coronary artery and *MEG3* is postulated to contribute to the development of hypoxia leading to cardiac cell death. An in vitro study using mouse H9c2 cells found that *MEG3* is upregulated under hypoxic conditions. *MEG3* in this scenario acts as a ceRNA, competing with TRPV4 for the binding of regulatory miRNA miR-325-3p. In healthy cells, miR-325-3p regulates TRPV4 keepings its expression low, however, under hypoxic conditions, *MEG3* upregulation outcompetes TRPV4, allowing for greater expression of TRPV4 which leads to cell death (*34*). Another study shows *MEG3* function as a ceRNA contributing to cardiac hypertrophy when the lncRNA is upregulated. This study demonstrates that *MEG3* binds to miR-361-5p, inhibiting its regulatory effect on histone deacetylase 9 (HDAC9). Increased expression of HDAC9 is associated with the progression of cardiac hypertrophy. The findings indicate that upregulation of *MEG3* leads to enhanced HDAC9 expression through the sponging of miR-361-5p, thereby promoting cardiac hypertrophy (*35*).

An example in which *MEG3* knockdown is beneficial and alleviates disease pathology is in hyperhomocysteinemia, a medical condition characterized by abnormally high levels of homocysteine in the blood, which is associated with an increased risk of cardiovascular diseases. Using mouse cardiac fibroblasts, researchers injected homocysteine to model an environment prone to cardiac disease. Then treating cells with Selenium (Se) which is an essential trace element with antioxidant properties that mitigates oxidative stress and inflammation they saw that Se downregulated *MEG3* which significantly inhibited homocysteine -induced activation of the JAK2/STAT3 pathway, which is associated with cardiac fibroblast inflammation and oxidative stress. *MEG3* knockdown using a shRNA also led to a decrease in activation of the JAK2/STAT3 pathway (*36*). These studies highlight the potential of targeting *MEG3* for knockdown as a therapeutic strategy in cardiac disease. This adds an important dimension to my research, as my gapmers can effectively knock down all transcript variants of *MEG3*, opening avenues for treatment in various other diseases.

Although the experimental results are promising, a significant limitation is the use of fibroblasts as a model for human neuronal cells. While the efficacy of gapmers is relevant for both fibroblasts and neurons, since they target conserved regions capable of knocking down all transcript variants of *MEG3*, the significant differences in *MEG3* expression between these cell types may suggest different functional roles (*10*). This variation in function could help explain why both the non-target control and Oligo12 had the same effect on necrosome expression after TNF treatment. The mechanism of fibroblast necroptosis and AD neuronal may differ and *MEG3* might not be necessary for activation as found in De Strooper., et al. To further test my gapmers and the effect *MEG3* knockdown has on AD necroptosis I would use an improved model. A strong model to mimic

neuronal necroptosis in AD comes from (*37*) which cultures microglia stimulated with toxic amyloid beta oligomers for 48hrs. Then the media from this is used to culture neuronal cells, mimicking the toxic environment created by stimulated microglia, activating necroptosis in these cells. This model would provide a better platform to test the effect of my gapmers rescuing cells from necroptosis. Another area of this experiment which requires optimization to improve the data is to measure the phosphorylation states of RIPK1, RIPK3 and MLKL. Although previous work has shown necroptosis increases expression of these genes through qPCR, the main indication of their activation is by their phosphorylation state. The necrosome is formed when these proteins are phosphorylated, so by Western Blotting these proteins will give a better indication of the necessary modifications that occur during necroptosis and if the gapmers can reduce the post-translation modifications (*21, 22*).

On the other hand, away from neurodegeneration, many oncology studies have been investigating *MEG3* and its critical role in cancer biology, as downregulation of this lncRNA has been associated with a variety of cancers (*38, 39, 40*). *MEG3* is essential for maintaining cellular homeostasis and preventing the progression of cancer. Its key functions include inhibiting cell growth, regulating the cell cycle, inducing apoptosis, preventing metastasis, inhibiting angiogenesis, and suppressing the epithelial-to-mesenchymal transition (*39*). By performing these functions, *MEG3* acts as a crucial regulator of cellular behaviour, ensuring that cells respond appropriately to internal and external signals. Typically, *MEG3* controls these functions by functioning as a competing endogenous RNA (ceRNA), modulating the activity of miRNAs (*38, 39*). When *MEG3* is significantly downregulated, these vital functions are compromised, leading to uncontrolled cellular proliferation and tumorigenesis. This must be carefully considered when developing *MEG3*-based therapies, as extensive knockdown of all *MEG3* transcript variants could pose risks to off-target tissues, such as the ovaries, breasts, bladder, and lungs, which are susceptible to cancer through *MEG3* downregulation.

Due to downregulation leading to cancer, understanding the transcriptome of *MEG3* in AD and cells prone to cancer is vital for progressing therapies that knockdown *MEG3* expression. LncRNAs typically have diverse transcription patterns between cell types and these transcriptional differences leads to different functions (*41, 42*). *MEG3* has 19 known transcript variants, yet the transcription selectivity for each cell type is not known. De Strooper., et al., found that exon 2 was the most abundant transcript variant in the AD mice model, whether this is true for other cell types needs to be studied. I would start by investigating how *MEG3* activates necroptosis and if a specific transcript variant performs this task. This sets up a specific target that could allow only targeting of the dysfunctional *MEG3* transcript variant that leads to neurodegeneration through necroptosis, leaving other variants of *MEG3* to perform their necessary functions to maintain cell health. This could be done by cloning an array of *MEG3* plasmid for each specific transcript variant and assess cell death in human-derived H9 cells like in De Strooper., et al. From here I would need to assess if the transcript variant leading to necroptosis also partake in cancer pathology. This

could be achieved by performing RNA-sequencing on various cancer cell lines and transfecting the *MEG3* transcript variant plasmids to see if there is a gain-of-function which leads to the cancer pathology for that cell line. This type of work would give a better understanding of *MEG3* transcript variation and function, and how these changes can lead to disease. Additionally, it would help refine my knockdown selection to target only the necessary transcripts. This added specificity would reduce the risk of off-target effects from the treatment, helping to prevent unintended disease from the therapy.

Conclusion

My research provides an optimized method to knock down *MEG3* for use in diseases where upregulation leads to pathology, such as AD and neurodegenerative disease. The choice of gapmer oligonucleotides targeting conserved regions, specifically exons 2 and 3, led to a potent knockdown of *MEG3*, significantly more effective than any method previously used. The effectiveness of the gapmers was demonstrated through IC50 analysis, which indicated that significant knockdown can be achieved at very low doses. This finding enhances both the therapeutic safety and potential of the treatment, suggesting that lower doses could minimize side effects while maximizing efficacy. Although I was unable to replicate the results of De Strooper., et al., by rescuing cells from necroptosis through *MEG3* knockdown alone, this can be explained by the experimental method used and does not undermine the important role *MEG3* plays in activating necroptosis, as this paper established. This research paves the way for further exploration of *MEG3*'s role in necroptosis, as well as a deeper understanding of the different functions of its transcript variation. Ultimately, the goal is to develop therapeutics that specifically target *MEG3* to alleviate neuronal necroptosis without affecting other pathways, ensuring a focused approach in therapeutic applications.

References

1) Crick, F. (1970). Central dogma of molecular biology. *Nature*, **227**(5258), 561-563. https://doi.org/10.1038/227561a0.
2) International Human Genome Sequencing Consortium. (2001). Initial sequencing and analysis of the human genome. *Nature*, **409**(6822), 860-921. https://doi.org/10.1038/35057062.
3) Huang, B., and Zhang, R. (2014). Regulatory non-coding RNAs: Revolutionizing the RNA world. *Molecular Biology Reports*, **41**, 3915-3923. https://doi.org/10.1007/s11033-014-3259-6.
4) Brannan, C. I., Dees, E. C., Ingram, R. S., and Tilghman, S. M. (1990). The product of the H19 gene may function as an RNA. *Nature*, **347**, 669-671. https://doi.org/10.1038/347669a0.
5) Brockdorff, N., Ashworth, A., and Kay, G. F. (1991). The mouse Xist gene: A candidate for the X chromosome inactivation centre. *Nature*, **351**, 329-331. https://doi.org/10.1038/351329a0.

6) Gregory, T. R. (2001). The G-value paradox and the evolution of genome size. *Evolutionary Biology*, **32**, 233-248. https://doi.org/10.1007/s11692-001-0014-5.
7) Quinn, J., and Chang, H. (2016). Unique features of long non-coding RNA biogenesis and function. *Nature Reviews Genetics*, **17**, 47-62. https://doi.org/10.1038/nrg.2015.10.
8) Zhou, Y., Zhang, X., and Klibanski, A. (2012). *MEG3* noncoding RNA: A tumor suppressor. *Journal of Molecular Endocrinology*, **48**(3), R45-R53. https://doi.org/10.1530/JME-12-0008.
9) Meyer, K. D., & Jaffrey, S. R. (2014). The importance of m6A methylation in the regulation of gene expression. *Nature Reviews Molecular Cell Biology*, **15**(6), 313-326. https://doi.org/10.1038/nrm.2014.3.
10) National Center for Biotechnology Information. (2024). *MEG3 gene*. Retrieved from https://www.ncbi.nlm.nih.gov/gene/55384.
11) Dunn-Davies, H., et al. (2024). Control of endothelial cell function and arteriogenesis by *MEG3*: EZH2 epigenetic regulation of integrin expression. *Molecular Therapy - Nucleic Acids*, **35**, 102173. https://doi.org/10.1016/j.omtn.2024.102173
12) Peng, W., et al. (2015). Long non-coding RNA *MEG3* functions as a competing endogenous RNA to regulate gastric cancer progression. *Journal of Experimental & Clinical Cancer Research*, **34**, 79. https://doi.org/10.1186/s13046-015-0197-7.
13) Yan, H., et al. (2017). Long non-coding RNA *MEG3* functions as a competing endogenous RNA to regulate ischemic neuronal death by targeting the miR-21/PDCD4 signaling pathway. *Cell Death & Disease*, **8**, 3211. https://doi.org/10.1038/s41419-017-0047-y.
14) Zhou, Y., et al. (2007). Activation of p53 by *MEG3* non-coding RNA. *Journal of Biological Chemistry*, **282**(34), 24731-24742. https://doi.org/10.1074/jbc.M702029200.
15) Alzheimer's Association**.** (2023). 2023 Alzheimer's disease facts and figures. *Alzheimer's & Dementia*, **19**(1), 1-42. https://doi.org/10.1002/alz.12656.
16) Reitz, C., & Mayeux, R. (2014). Alzheimer disease: Epidemiology, diagnostic criteria, risk factors, and biomarkers. *Biochemical Pharmacology*, **88**(4), 640-651. https://doi.org/10.1016/j.bcp.2014.05.008.
17) Mullard, A. (2016). Alzheimer's drugs fail in phase III trials. *Nature Reviews Drug Discovery*, **15**(12), 755-757. https://doi.org/10.1038/nrd.2016.158.
18) van Dyck, C. H., et al. (2016). Lecanemab in early Alzheimer's disease. *New England Journal of Medicine*, **388**, 27-39. https://doi.org/10.1056/NEJMoa2202853.
19) De Strooper, B., et al. (2023). *MEG3* activates necroptosis in human neuron xenografts modeling Alzheimer's disease. *Science*, **381**, 1176-1182. https://doi.org/10.1126/science.abp9556.
20) Costigan, A., Hollville, E., and Martin, S. J. (2023). Discriminating between apoptosis, necrosis, necroptosis, and ferroptosis by microscopy and flow cytometry. *Current Protocols*, **3**, e951. https://doi.org/10.1002/cpz1.951.
21) Pasparakis, M., and Vandenabeele, P. (2015). Necroptosis and its role in inflammation. *Nature*, **517**, 311-320. https://doi.org/10.1038/nature14139.
22) Seo, J., et al. (2021). Necroptosis molecular mechanisms: Recent findings regarding novel necroptosis regulators. *Experimental & Molecular Medicine*, **53**, 1007-1017. https://doi.org/10.1038/s12276-021-00634-7.
23) Khoury, Mitri K., et al. "Necroptosis in the Pathophysiology of Disease." The American Journal of Pathology, vol. 190, no. 2, 2020, pp. 272-285. ISSN 0002-9440, https://doi.org/10.1016/j.ajpath.2019.10.012.
24) Zhang, H. (2019). Mechanism associated with aberrant lncRNA *MEG3* expression in gestational diabetes mellitus. *Experimental and Therapeutic Medicine*, **18**, 3699-3706. https://doi.org/10.3892/etm.2019.8062.

25) Selkoe, D. J., & Hardy, J**.** (2016). The amyloid hypothesis of Alzheimer's disease at 25 years. *EMBO Molecular Medicine*, **8**(6), 595-608. https://doi.org/10.15252/emmm.201606210.
26) Cai, Z., et al. (2020). The role of inflammation in Alzheimer's disease: A review. *Frontiers in Aging Neuroscience*, **12**, 111. https://doi.org/10.3389/fnagi.2020.00111.
27) Khalil, A. M., et al**.** (2009). Many human large intergenic non-coding RNAs overlap with known protein-coding genes. *Nature*, **457**, 185-191. https://doi.org/10.1038/nature07640.
28) Maruyama, R., and Yokota, T. (2020). Knocking down long noncoding RNAs using antisense oligonucleotide gapmers. In *Gapmers*, T. Yokota and R. Maruyama, eds. Methods in Molecular Biology, **2176**, 45-58. https://doi.org/10.1007/978-1-0716-0771-8_3.
29) Chan, L., and Yokota, T. (2020). Development and clinical applications of antisense oligonucleotide gapmers. In *Gapmers*, T. Yokota and R. Maruyama, eds. Methods in Molecular Biology, **2176**, 27-44. https://doi.org/10.1007/978-1-0716-0771-8_2.
30) Gonzalez, M. M., et al. (2021). The necrosome gene expression signature is a potential biomarker for necroptosis in multiple diseases. *Cell Death & Disease*, **12**, 11. https://doi.org/10.1038/s41419-021-03876-6.
31) Zhang, Y., et al. (2019). Evaluation of the cytotoxicity of lipofectamine 2000 in cultured cells. *Journal of Biomolecular Techniques*, **30**(1), 20-30.
32) Li, J., et al. (2023). The multifaceted biology of lncR-*MEG3* in cardio-cerebrovascular diseases. *Frontiers in Genetics*, **14**, 1132884. https://doi.org/10.3389/fgene.2023.1132884.
33) Zhang, Y., et al. (2021). Long non-coding RNA *MEG3*: A potential therapeutic target in cardiovascular disease. *Frontiers in Pharmacology*, **12**, 645992. https://doi.org/10.3389/fphar.2021.645992.
34) Zhou, Y., et al. (2021). Long non-coding RNA *MEG3* knockdown alleviates hypoxia-induced injury in rat cardiomyocytes via the miR-325-3p/TRPV4 axis. *Molecular Medicine Reports*, **23**(1), 18. https://doi.org/10.3892/mmr.2020.11656.
35) Zhang, J., Liang, Y., Huang, X., et al. (2019). STAT3-induced upregulation of lncRNA *MEG3* regulates the growth of cardiac hypertrophy through the miR-361-5p/HDAC9 axis. *Scientific Reports*, **9**, 460. https://doi.org/10.1038/s41598-018-36369-1.
36) Li, W., et al. (2021). Se alleviates homocysteine-induced fibrosis in cardiac fibroblasts via downregulation of lncRNA *MEG3*. *Experimental and Therapeutic Medicine*, **22**, 1269. https://doi.org/10.3892/etm.2021.10704.
37) Salvadores, N., et al. (2022). Aβ oligomers trigger necroptosis-mediated neurodegeneration via microglia activation in Alzheimer's disease. *Acta Neuropathologica Communications*, **10**, 31. https://doi.org/10.1186/s40478-022-01332-9.
38) Al-Rugeebah, A., Alanazi, M., and Parine, N. R. (2019). *MEG3*: An oncogenic long non-coding RNA in different cancers. *Pathology & Oncology Research*, **25**(2), 859–874. https://doi.org/10.1007/s12253-019-00614-3.
39) Zhang, L., et al. (2022). The biological roles and molecular mechanisms of long non-coding RNA *MEG3* in the hallmarks of cancer. *Cancers*, **14**(24), 6032. https://doi.org/10.3390/cancers14246032.
40) He, Y., et al. (2017). Potential applications of *MEG3* in cancer diagnosis and prognosis. *Oncotarget*, **8**(42), 73282-73295. https://doi.org/10.18632/oncotarget.19931.
41) Gao, Y., et al. (2021). Long non-coding RNAs: new players in the regulation of gene expression. *Frontiers in Genetics*, **12**, 621053. https://doi.org/10.3389/fgene.2021.621053.
42) Guttman, M., and R. S. Young**.** (2013). RNA networks in gene regulation. *Nature Reviews Molecular Cell Biology*, **14**, 285-298. https://doi.org/10.1038/nrm3563.

43) Naito, Y., & Nakayama, M. (2014). GGGenome ultrafast DNA search: A tool for rapid off-target screening of nucleic acid-based therapeutics. *Bioinformatics*. https://gggenome.dbcls.jp/.
44) Hagedorn, P. H., et al. (2018). Identifying and avoiding off-target effects of RNase H-dependent antisense oligonucleotides in mice. *Nucleic Acids Research, 46*(11), 5366–5380. https://doi.org/10.1093/nar/gky397.
45) Freitas, G. A., & Niswender, C. M. (2023). GRM7 gene mutations and consequences for neurodevelopment. *Pharmacology Biochemistry and Behavior, 225*, 173546. https://doi.org/10.1016/j.pbb.2023.173546
46) Love-Gregory, L., & Permutt, M. A. (2007). HNF4A genetic variants: Role in diabetes. *Current Opinion in Clinical Nutrition and Metabolic Care, 10*(4), 397–402. https://doi.org/10.1097/MCO.0b013e3281e3888d
47) Hommersom, M. P., et al. (2022). The complexities of CACNA1A in clinical neurogenetics. *Journal of Neurology, 269*(9), 3094–3108. https://doi.org/10.1007/s00415-021-10902-3
48) Dustin, D., Gu, G., & Fuqua, S. A. W. (2019). ESR1 mutations in breast cancer. *Cancer, 125*(21), 3714–3728. https://doi.org/10.1002/cncr.32345
49) Anwar, S., Mir, F., & Yokota, T. (2023). Enhancing the effectiveness of oligonucleotide therapeutics using cell-penetrating peptide conjugation, chemical modification, and carrier-based delivery strategies. *Pharmaceutics, 15*(4), 1130. https://doi.org/10.3390/pharmaceutics15041130

Figures and Tables

Gapmer	Target	Sequence (5'-3')	GC%	Off-target hits	Self-complementary	Melting Temperature (ºC)
NTC1	N/A	AGCGT – TTAGGCTATG – TACTT	40	NG_030354.1	No	59.9
Oligo1	Exon2	TGTCA – TCCCTGAGGA – GACAC	55	None	No	66.2
Oligo2	Exon2	GAGGT – GGACGGATGA – TGTCA	55	None	No	65.1
Oligo3	Exon2	AGGTG – GTCCTTGAAG – ACAAG	50	None	No	63.8
Oligo4	Exon2	AGCAG – CTCAGCATGG – AGAGG	60	None	No	68.4
Oligo5	Exon2	GCAGC – AGGCCCCTTG – GCAGC	75	None	No	76.1
Oligo6	Exon2	CGTGA – GGTGTAGATG – GGCAG	60	None	No	67.5
Oligo7	Exon3	AGGAA – ACCGTGCTCC – TAGTG	55	None	No	66.4
Oligo8	Exon3	TTGTA – TGTTGGTGGG – ATCCA	45	None	No	62.7
Oligo9	Exon3	CCTTT – GCCATCCTGG – TCCTG	60	None	No	67.9
Oligo10	Exon3	GCTGG – TCAGTTCCGG – TCCTC	65	None	No	69.9
Oligo11	Exon3	AGGGC – ATTGGTTTAA – GTCTT	40	None	No	59.7
Oligo12	Exon3	TTAGG – TAAGAGGGAC – AGCTG	50	[Table 3]	No	65

Table 1: Properties of gapmers targeting MEG3. The table includes the gapmer name, target exon, sequence (5′ to 3′), GC content (%), off-target hits, self-complementarity, and melting temperature (°C).

Gapmer	Target	Sequence (5'-3')	GC%	Off-target hits	Self-	Melting Temperature

					complementary	(ºC)
Oligo13	Exon3	TGGGA - TCCAGGAAAC - CGTGC	60	None	No	68.5
Oligo14	Exon3	TGAGT- GGCTGCTTTG - TATGT	45	None	No	62.7
Oligo15	Exon3	ATCCA - GGAAACCGTG - CTCCT	55	None	No	66.9
Oligo16	Exon3	TTGGT- GGGATCCAGG - AAACC	55	None	No	66.7
Oligo17	Exon3	TATGT - TGGTGGGATC - CAGGA	50	None	No	65.5
Oligo18	Exon3	TGCTT - TGTATGTTGG - TGGGA	45	None	No	62.9
Oligo19	Exon3	TGAGT - GGCTGCTTTG - TATGT	45	None	No	62.7
Oligo20	Exon3	TCAGT - GAGTGGCTGC - TTTGT	50	None	No	65.2
Oligo21	Exon3	GGGGT - CAGTGAGTGG - CTGCT	65	None	No	72.1
Oligo22	Exon3	TCCTG - GGGGTCAGTG - AGTGG	65	None	No	72.2
Oligo23	Exon3	CTGGT - CCTGGGGGTC - AGTGA	65	None	No	72.1
Oligo24	Exon3	CATCC - TGGTCCTGGG - GGTCA	65	None	No	72
Oligo25	Exon3	TTGCC - ATCCTGGTCC - TGGGG	65	None	No	72.1

Table 2: Properties of gapmers targeting MEG3. The table includes the gapmer name, target exon, sequence (5′ to 3′), GC content (%), off-target hits, self-complementarity, and melting temperature (°C).

Gene ID	Gene name	Sequence	Binding	Matches	% Identity	Score	E-value
NM_000844.4	GRM7	TT-GGTAAGAGGGAAAGCCG	Intron	17	85	16	0.002941
NM_001004196.4	CD200	TTACTT-AGAGGGACAGCTG	Intron	17	85	16	0.002941
NM_001004720.3	NCK2	TT-GGTAAGAGGGAAAGCCG	Intron	17	85	16	0.002941
NM_001009909.4	LUZP2	GTAGGTAAG-GGGACA-CTG	Intron	17	85	15	0.002941
NM_001030003.3	HNF4A	TTAGGTAGGAGGGAAA-CTG	Exon	17	85	16	0.002941
NM_000044.6	AR	CTAGTTAA-AGGGACAACTG	Intron	16	80	15	0.003125
NM_000059.4	BRCA2	CCAGGT-AGAGGGACA-CTG	Intron	16	80	14	0.003125
NM_000068.4	CACNA1A	TTAGGAAGGAGGTGACAG-TG	Intron	16	80	14	0.003125
NM_000093.5	COL5A1	CTAGAGTGA-AGGGACAGCTG	Intron	16	80	14	0.003125
NM_000125.4	ESR1	TTAGCTAAGAGCAACATCTG	Intron	16	80	16	0.003125

Table 3: Summary of potential off-target sequences for Oligo 12. The table includes the gene ID, gene name, sequence alignment with mismatches (red), deletions ('-'), and insertions (green), binding region (intron or exon), number of matches, percentage identity, alignment score, and E-value.

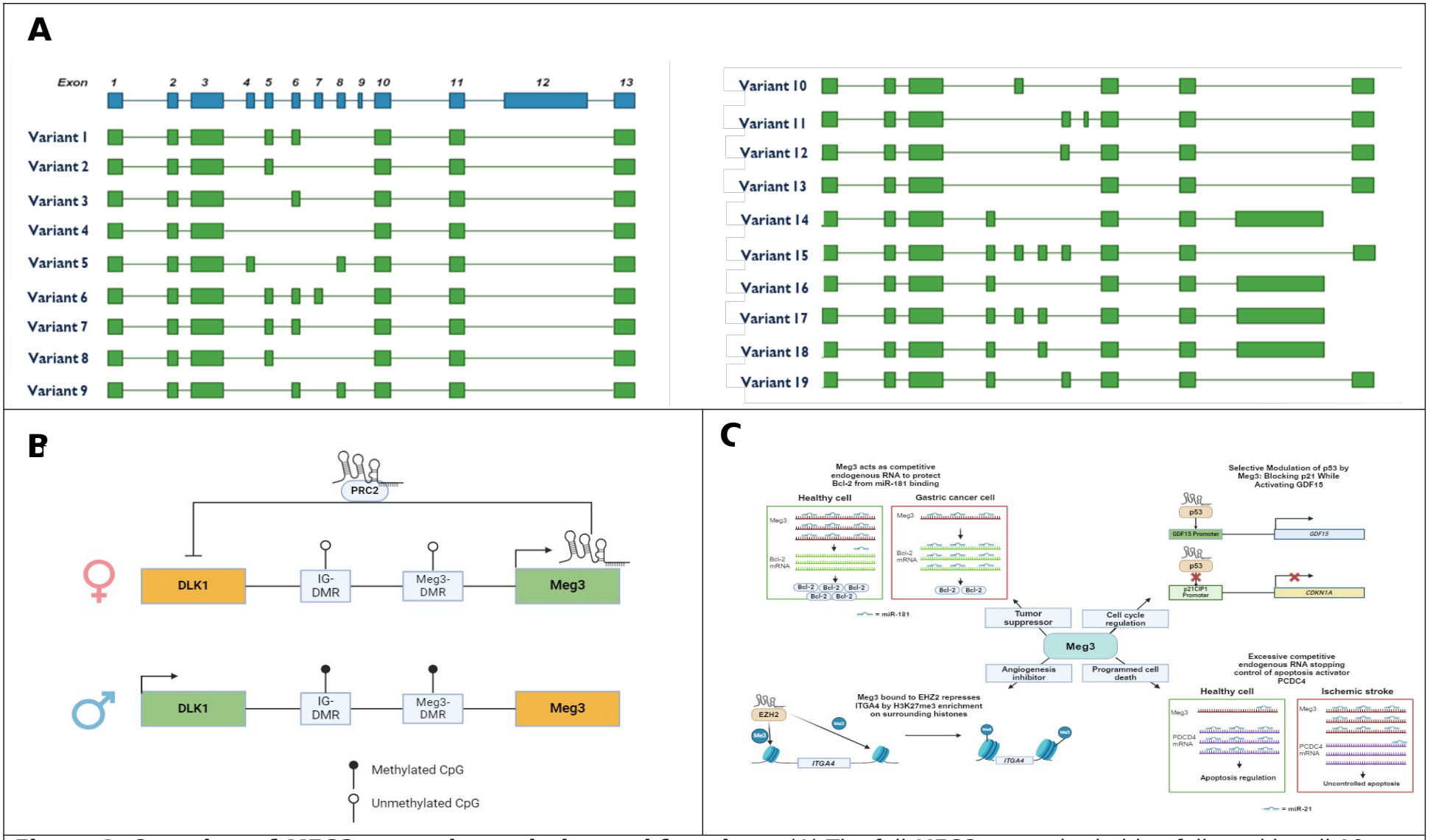


Figure 1: Overview of *MEG3* transcript variation and functions. (A) The full *MEG3* transcript in blue followed by all 19 transcript variants. (B) The mechanism of imprinting at the DLK1-*MEG3* locus. (C) A schematic of the four functions of *MEG3*

through its role as a ceRNA, performing chromtin remodelling, and binding transcription factors.

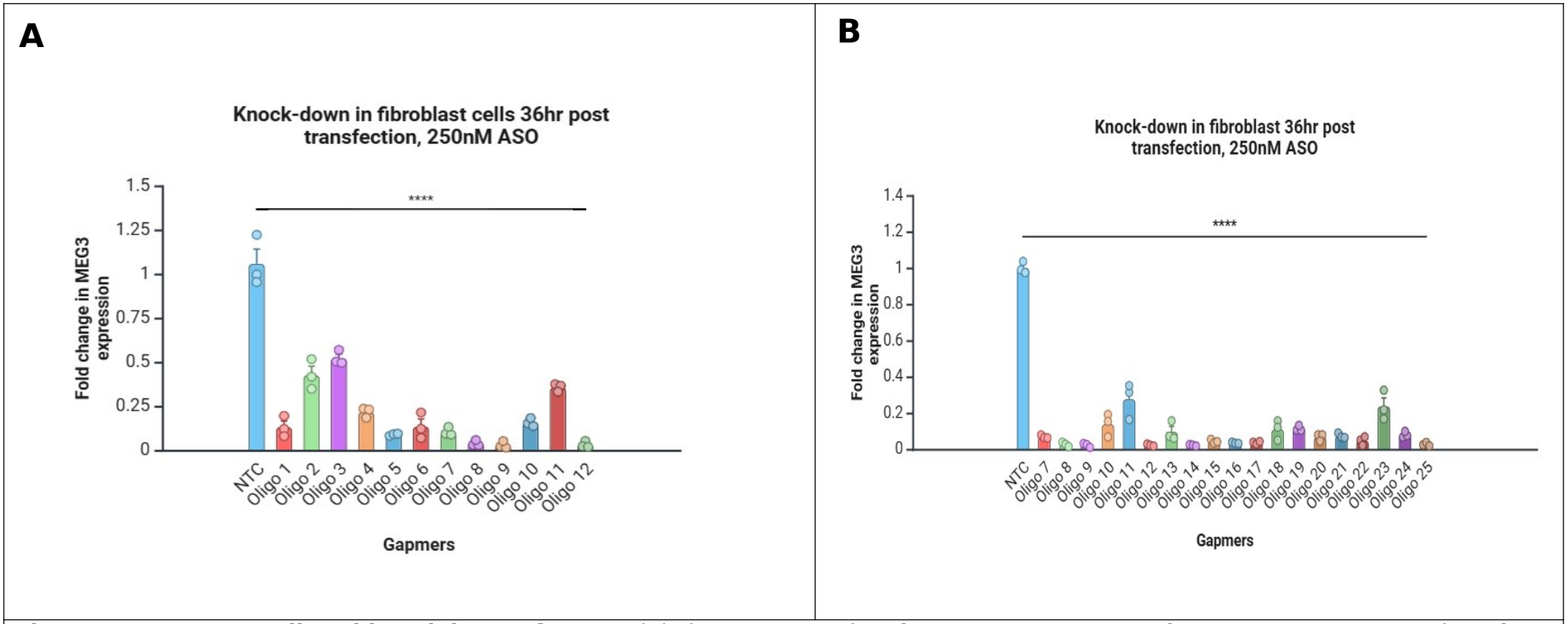


Figure 2: Gapmer mediated knockdown of *MEG3*. (A) First assay results of 12 gapmers. 250 nM of gapmer per treatment, kept for 36 hours. NTC used as calibrator treatement and TNP used as engodenous control. Fold change calcualted by Delta Delta Ct. (B) Second assay of gapmers which target exon3. Same method as (a). Significance: **** P-value < 0.0001.

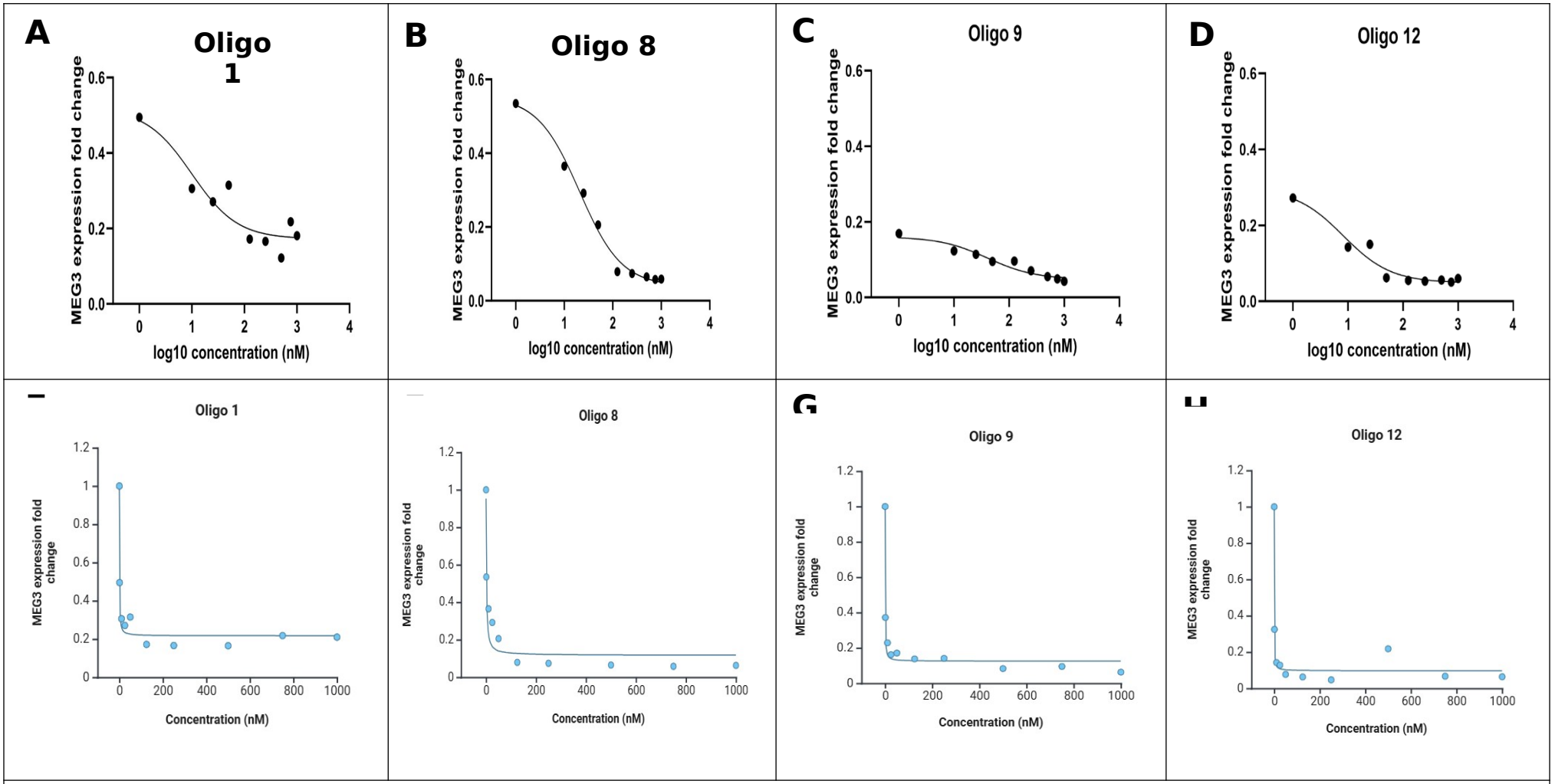


Figure 3: Gapmer mediated knockdown of *MEG3*. (A) Log10 concentration dose dependance response for Oligo 1 (B) Log10 concentration dose dependance response for Oligo 8. (C) Log10 concentration dose dependance response for Oligo 9. (D) Log10 concentration dose dependance response for Oligo 12. (E) Oligo 1 dose dependance response with projected regression curve. (F) Oligo 8 dose dependance response with projected regression curve. (G) Oligo 9 dose dependance response with projected regression curve. (H) Oligo 12 dose dependance response with projected regression curve

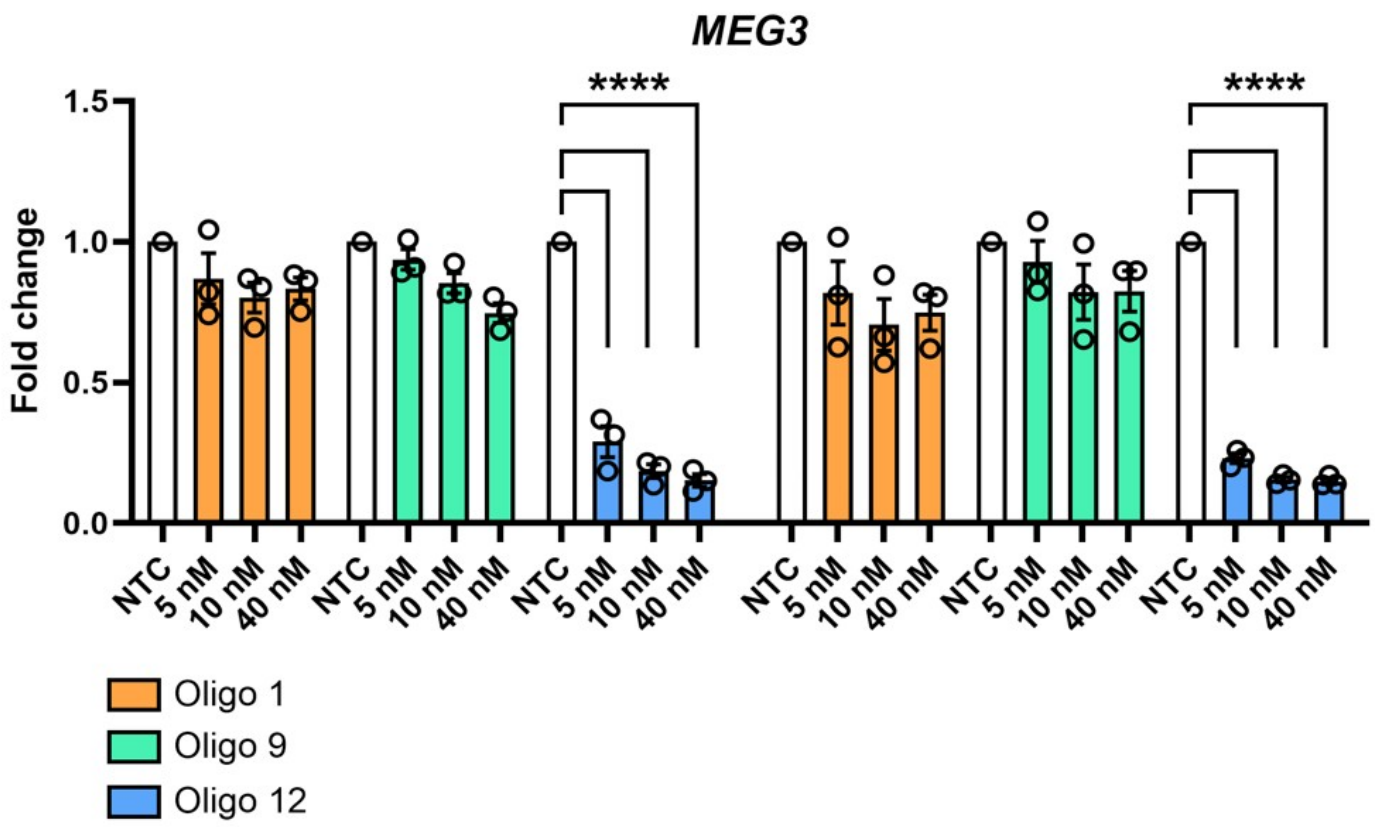


Figure 4: siRNA mediated knockdown of *MEG3*. (A) Oligo 1 (orange), 9 (green) and 12 (blue) tested in siRNA chemistry at three concentrations: 5 nM, 10 nM and 40 nM. Two timpoints, 36hrs on the left and 72hr on the right. *MEG3* fold change for each timepoint

normalied to NTC. Significance **** P-value < 0.0001.

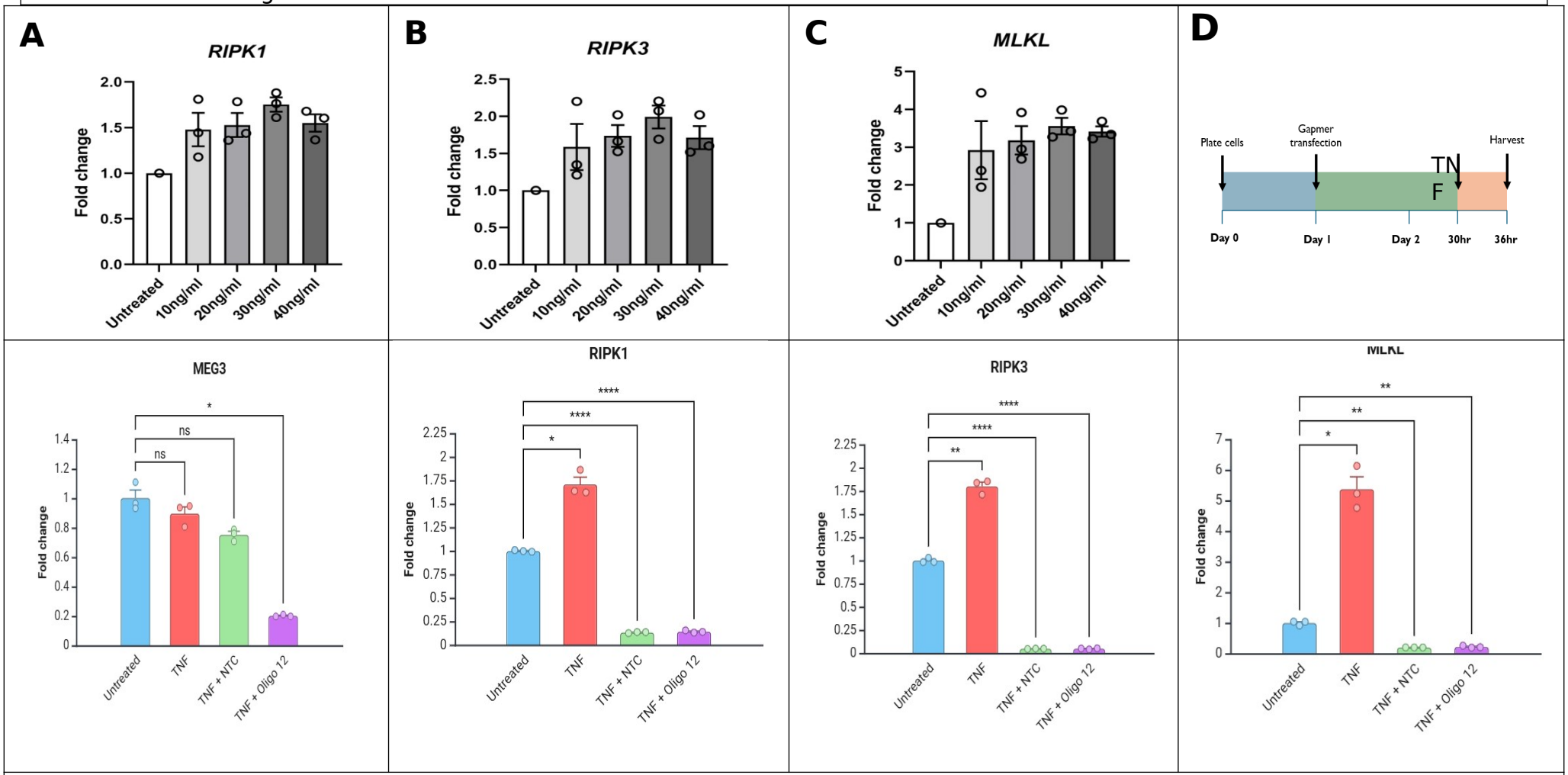


Figure 5: *In vitro* necroptosis indcuction and rescue. (A) Fold change in RIPK1 expression at increasing concentrations of TNF-alpha. Untreated used a calibrator and GAPDH as endogenous control. (B) Fold change in RIPK3 expression. Same method as (a). (C) Fold change in MLKL expression. Same method as (a). (D) Method used to rescue cells from necroptosis. (E) Fold change in *MEG3* expression post necroptosis revival. (F) Fold change in RIPK1 post necroptosis rescue. (G) Fold change in RIPK3 post necroptisis rescue.

(H) Fold change in MKLK post necroptosis rescue. Significance: * P-value = 0.0445, ** P-value = 0.004, *** P-value = 0.0003, **** P-value < 0.0001.